Thermally Induced Increase in Energy Transport Capacity of Silkworm Silks

Guoqing Liu,[1] Shen Xu,[1] Ting-Ting Cao,[2] Huan Lin,[1] Xiaoduan Tang,[1] Yu-Qing Zhang,[2] Xinwei Wang[1]

[1] *Department of Mechanical Engineering, Iowa State University, Ames 50011, Iowa*

[2] *Silk Biotechnology Key Laboratory of Suzhou City, School of Biology and Basic Medical Sciences, Soochow University, Suzhou 215123, People's Republic of China*

Received 28 October 2013; revised 7 April 2014; accepted 8 April 2014
Published online 11 April 2014 in Wiley Online Library (wileyonlinelibrary.com). DOI 10.1002/bip.22496

ABSTRACT:

This work reports on the first study of thermally induced effect on energy transport in single filaments of silkworm (Bombyx mori) fibroin degummed mild (type 1), moderate (type 2), to strong (type 3). After heat treatment from 140 to 220° C, the thermal diffusivity of silk fibroin type 1, 2, and 3 increases up to 37.9, 20.9, and 21.5%, respectively. Our detailed scanning electron microscopy study confirms that the sample diameter change is almost negligible before and after heat treatment. Raman analysis is performed on the original and heat-treated (at 147° C) samples. After heat treatment at 147° C, the Raman peaks at 1081, 1230, and 1665 cm^{-1} become stronger and narrower, indicating structural transformation from amorphous to crystalline. A structure model composed of amorphous, crystalline, and laterally ordered regions is proposed to explain the structural change by heat treatment. Owing to the close packing of more adjacent laterally ordered regions, the number and size of the crystalline regions of Bombyx mori silk fibroin increase by heat treatment. This structure change gives the observed significant thermal diffusivity increase by heat treatment. © 2014 Wiley Periodicals, Inc. Biopolymers 101: 1029–1037, 2014.

Correspondence to: Xinwei Wang; e-mail: xwang3@iastate.edu

Keywords: *silkworm silk; thermal treatment; thermal diffusivity; Raman spectroscopy*

This article was originally published online as an accepted preprint. The "Published Online" date corresponds to the preprint version. You can request a copy of the preprint by emailing the Biopolymers editorial office at biopolymers@wiley.com

INTRODUCTION

Silkworm silk from *Bombyx mori* has many advantages, such as comfort, high mechanical strength and elasticity,[1] and has been widely used in textile industry for thousands of years.[2] In the past century, this material also provided important clinical repair options for many applications, such as suture material.[3] With the development of biomedical and biotechnological engineering, it finds more and more applications in biosensors, drug delivery, etc.[2–5] It is well known that silkworm silk is a fibrous protein composed of two strands of fibroin coated with a layer of sericin. The sericin layer is usually removed for making regenerated silk-based devices. The properties of degummed silk (fibroin) fibers need to be fully characterized and recognized, and the thermal property is one of the most important properties.

In past studies, some works studied the changes of silkworm silk proteins' structures and mechanical properties by using thermal treatment,[6–8] and other thermal analysis of silk fibroins is focused on reconstituted silk fibroin (RSF) films,[2,9–11] not the native silks naturally produced by silkworms. For RSF films, there are various ways to induce structural changes (from amorphous to crystalline). For temperature-controlled water vapor annealing, the β-sheets crystallinity can increase

from 14% (when the water vapor annealing temperature is 4°C) to 57.8–59.6% (when the water vapor annealing temperature is 90–100°C).[12] For heat treatment, the original film is completely noncrystalline prior to the treatment. When heated above the glass transition temperature (T_g), the crystallinity can increase to 43% at 214°C.[2] Exposing to chemicals, such as ethanol and methanol can also affect the crystallization of β-sheets.[2,12,13]

The thermal transport properties, like thermal conductivity and thermal diffusivity, are highly affected by protein's molecular weight, alignment, crystallinity, defects, and secondary structure. So the thermal conductivity/diffusivity can be used to reflect the overall structural change of the protein fiber under heat treatment. For silks naturally produced by silkworms, due to the fact that the thickness of the single filament of protein fibers is only a few μm, very limited research about the thermal transport in these materials has been conducted. Attempts have been tried to measure the thermal properties in silkworm silks.[14] Silkworm silks show significant thermal transport improvement under stretching.

In this work, for the first time the effect of heat treatment on the thermal transport properties of silk fibroin fibers are fully investigated. For RSF films, many studies showed that when the samples are heated above the glass transition temperature (T_g), structural transformation from amorphous to crystalline can be induced. For RSF films, the glass transition temperature is about 178°C,[2,6,15,16] and for native silk fibroin from glands of silkworms, it ranges from 160 to 210°C.[9,17,18] At the same time, thermogravimetric studies of silk showed that thermal decomposition occurs in a broad temperature range beginning at about 197°C.[12,19,20] Taking all of these factors into consideration, the heat treatment temperature is set from ~140 to ~220°C in our experiment. Three types of fibroin fibers of *Bombyx mori* that are prepared by three kinds of degumming methods are studied. Raman analysis shows that the peaks at 1081, 1230, and 1665 cm^{-1} become sharper after the heat treatment at 147°C. A model of laterally ordered regions of the silk fibers is developed to explain the structural changes induced by the heat treatment.[7]

EXPERIMENT DETAILS

Sample Preparation

Three types of silk (*Bombyx mori*) fibroin fibers are prepared by three kinds of degumming methods. The solutions used in this work are neutral soap, strongly alkaline electrolyzed water and Na_2CO_3 solution.

Type 1 Fiber. A known weight of clean cocoon shells is added into a 0.2% (W/V) neutral soap solution at a ratio of 1:100 (W/V) and heated at 100°C for 30 min. The neutral soap solution is removed, replaced with a fresh solution and heated again at 100°C for 30 min. This process is repeated four times. The degummed silk fibroin is washed repeatedly with about 40°C deionized water. The degummed silk fibroin fibers are also washed repeatedly and air-dried at 105°C for 2 h.

Type 2 Fiber. pH 11.50 strongly alkaline electrolyzed water is used for degumming cocoons. A 2.00 g sample (dry cocoon shells) is mixed with the electrolyzed water (pH 11.50) in a flask at a ratio of 1:40 (W/V). The flask is placed in a boiling water bath (100°C) for 20 min with constant stirring (120 rpm). The degummed silk fibroin fibers from the alkaline electrolyzed water are washed with deionized water and finally air-dried at 105°C for 2 h.

Type 3 Fiber. A known weight of clean cocoon shells is immersed in 0.5% (W/V) Na_2CO_3 at a ratio of 1:20 (W/V) and then heated for 30 min at 98°C. The resulting degummed silk is rinsed repeatedly (the washing water was kept) with 40°C deionized water then heated again for 30 min at 98°C in 0.5% Na_2CO_3. The degummed silk fibroin is washed repeatedly with about 40°C deionized water to ensure complete removal of the sericin surrounding the silk fibroin fiber. After washing repeatedly with deionized water, the degummed silk fibroin fibers are air-dried at 105°C for 2 h and then weighed.

Heat Treatment

After initial thermal characterization, silk fibroin fibers are heated in a bench-top muffle furnace (OMEGALUX LMF-A550) at about 140, 160, 180, and 220°C for 30 min, respectively. In order to improve the temperature measurement accuracy, a separate thermocouple has been placed in the chamber to monitor the inside temperature. After heat treatment, the samples are cooled down at room temperature for about 30 min before transferred to a vacuum chamber for thermal properties characterization.

Thermal Characterization

In this work, the transient electro-thermal (TET) technique is used to characterize the thermophysical properties of silkworm silks. The TET technique[21] is an effective approach developed to measure the thermal diffusivity of solid materials, including conductive, semiconductive or nonconductive one-dimensional structures. This technique has been used for successful thermal characterization of free-standing micrometer-thick poly (3-hexylthiophene) films,[22] thin films composed of anatase TiO_2 nanofibers,[23] single-walled carbon nanotubes,[21]

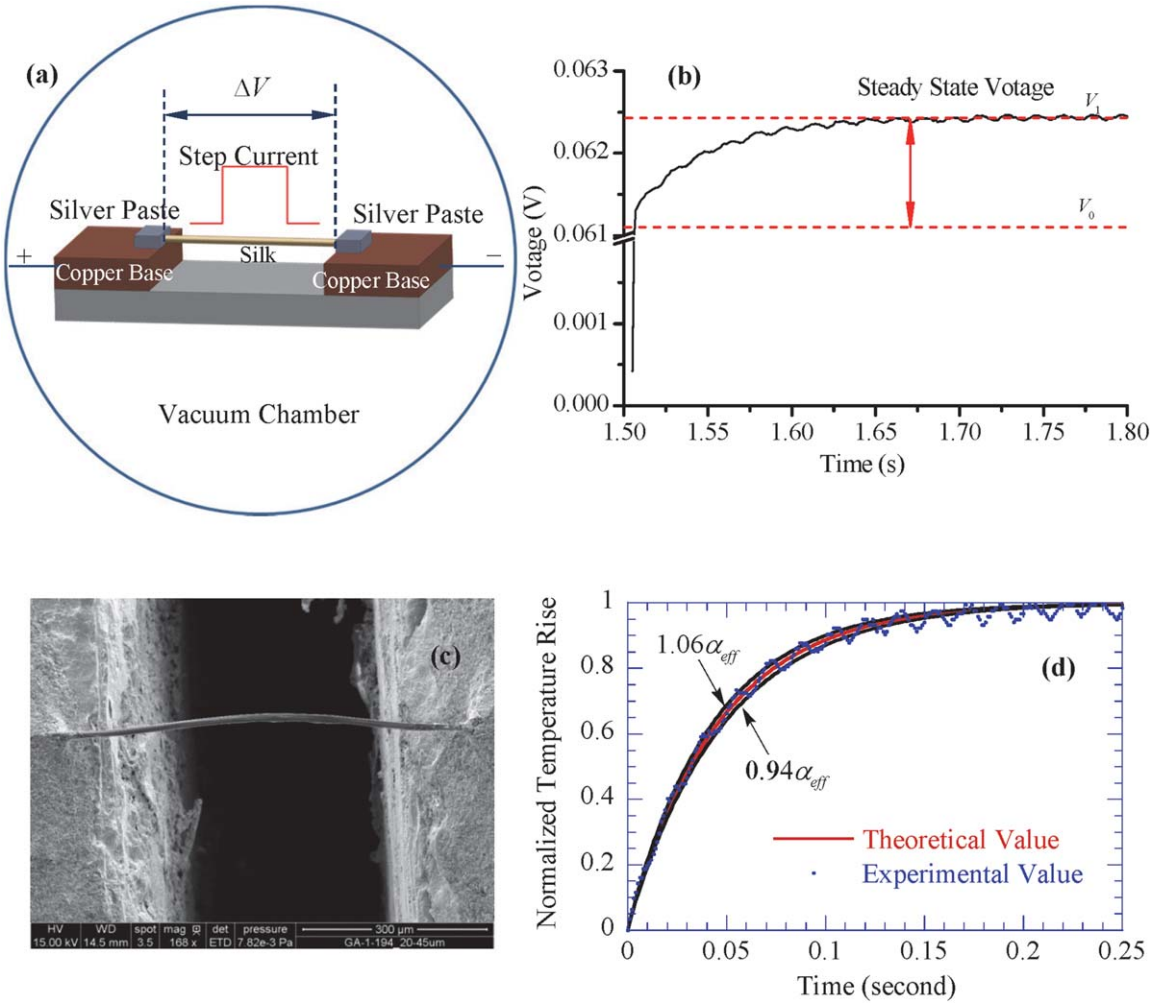

FIGURE 1 (a) Schematic of the experimental principle and the step current provided for the TET technique. (b) The methodology to determine the thermophysical properties based on the resulted $V-t$ profile (silk fibroin fiber Type 2). (c) A typical SEM image for silk fibroin fiber (Type 2). (d) Comparison between the theoretical fitting and experimental data for the normalized temperature rise versus time (silk fibroin fiber Type 2, before heat treatment).

micro/submicroscale polyacrylonitrile wires,[24] and protein fibers (silkworm silk).[14]

A schematic of the TET experiment setup is shown in Figure 1a. In the measurement, the sample is suspended between two copper electrodes. Silver paste is applied at the sample–electrode contact to reduce the thermal and electrical contact resistances to a negligible level. The whole sample is housed in a vacuum chamber to reduce the heat transfer to the air. During measurement, a step current is fed through the sample to induce joule heating. Because silk fibroin fibers are not electrically conductive, a very thin gold film (∼nm) is coated outside the sample to make it electrically conductive. The induced voltage–time (V–t) profile recorded by the oscilloscope is shown in Figure 1b. Upon this step current joule heating, the sample will experience a quick temperature increase. How fast/slow the temperature increases is determined by two competing processes: one is the joule heating, and the other one is the heat conduction from sample to electrodes. A higher thermal diffusivity of the sample will lead to a faster temperature evolution, meaning a shorter time to reach the steady state. Therefore, the transient voltage/temperature change can be used to determine the thermal diffusivity. When determining thermal diffusivity of the sample, no real temperature rise is needed. In fact, only the normalized temperature rise based on the voltage increase is used. The processes for determining the thermal diffusivity and thermal conductivity are outlined below.

During TET thermal characterization, the surface radiation effect could be significant if the sample has a very large aspect

ratio (L/D, L: sample length, D: sample diameter), especially for samples of low thermal conductivity. By converting the surface radiation and gas conduction to body cooling source, the heat transfer governing equation for the sample is:

$$\frac{1}{\alpha}\frac{\partial\theta(x,t)}{\partial t}=\frac{\partial^2\theta(x,t)}{\partial x^2}+\frac{I^2R_0}{kLA_c}+\frac{1}{k}\frac{16\varepsilon_r\sigma T_0{}^3}{D}\theta \tag{1}$$

where $\theta = T - T_0$, and T_0 the temperature of the environment (vacuum chamber). For rest parameters, α, R_0, σ, and ε_r are the thermal diffusivity, electrical resistance, the Stefan–Boltzmann constant and the effective emissivity of the sample, respectively. I is the current fed through the sample. k is the thermal conductivity of the fiber. A_c is the cross-sectional area, and equals to $\pi D^2/4$ (D: sample's diameter). This equation is derived based on $\theta \ll T_0$, which holds for most situations in our experiment. Defining $f=-(16\varepsilon_r\sigma T_0{}^3/D)\cdot L^2/\pi^2 k$ and with $\alpha_{eff}=\alpha(1-f)$, the normalized temperature rise (averaged over the sample) T^* can be expressed as

$$T^*\cong\frac{48}{\pi^4}\sum_{m=1}^{\infty}\frac{1-(-1)^m}{m^2}\frac{1-\exp\left[-m^2\pi^2\alpha_{eff}\,t/L^2\right]}{m^2} \tag{2}$$

Numeric calculations have been conducted to confirm the accuracy of the above solution. So we have

$$\alpha=\alpha_{eff}-\frac{1}{\rho c_p}\frac{16\varepsilon_r\sigma T_0{}^3}{D}\frac{L^2}{\pi^2} \tag{3}$$

where ρc_p is volume-based specific heat. The normalized temperature rise T^*_{exp} based on the experimental data can be calculated as $T^*_{exp}=(V_{wire}-V_0)/(V_1-V_0)$, where V_0 and V_1 are the initial and final voltages across the sample (shown in Figure 1b). In our work, after . is obtained, different trial values of α_{eff} are used to calculate the theoretical T^* using Eq. (2) and fit the experimental results (T^*_{exp}). The value giving the best fit of T^*_{exp} is taken as the effective thermal diffusivity of the sample. Then Eq. (3) is used to calculate the real thermal diffusivity of the sample. For the radiation effect, in our previous work, we have already determined the value of effective emissivity ε_r, which is 0.92.

This determined thermal diffusivity (α) in Eq. (3) has the gold effect. The thermal transport effect caused by the coated layer can be subtracted using the Wiedemann–Franz law with negligible uncertainty. The real thermal diffusivity (α) of the sample finally is determined as:[21]

$$\alpha_{real}=\alpha-\frac{L_{Lorenz}\,TL}{RA(\rho c_p)} \tag{4}$$

It can be obtained from calibration, noncontact photothermal technique or measuring the density and specific heat separately. L_{Lorenz} is the Lorenz number. Our previous study of gold films on glass fiber has revealed that the film has nanocrystalline structure. Its Lorenz number is 7.44×10^{-8} W Ω K^{-2}, significantly larger than the bulk value.[25] To further understand the effect of the gold film on the silkworm silk, we have coated a silkworm silk with gold film of different thickness and studied how the effective thermal diffusivity varies against the gold film thickness. Combining Eqs. (3) and (4), we have determined the Lorenz number as 2.10×10^{-8} W Ω K^{-2}. It is much smaller compared with the result for gold film on glass fibers since electron tunneling and hopping effect happens between gold films and silks. The hopping conduction increases the electron transport and electrical conductivity in the thin gold film, though there may be some tiny cracks in the gold film. Therefore, the Lorenz number on the silkworm silk is reduced and this number is used to subtract the gold effect in this work. Details of this gold film effect measurement will be published in our other work.

RESULTS AND DISCUSSION

TET Measurement and Uncertainty

To offer a general idea about the experimental procedure, here we discuss how to use the TET technique to characterize the thermal properties of a specific silk fibroin fiber (Type 2). After fixed on two copper bases with silver paste (Figure 1c), the fiber is coated with a thin layer of gold (about 40 nm) to make it electrically conductive. Then the sample is placed in a vacuum chamber, which is pumped down to about 1–3 mTorr. At this pressure, the gas conduction is negligible. A step DC current (0.7 mA) is fed through the sample to induce joule heating. The voltage evolution in one heating period (Figure 1b) is recorded by an oscilloscope. The voltage related to the temperature increases gradually to a constant indicating the temperature evolution from transient state to steady state. Based on the voltage evolution, the normalized temperature rise of the sample is calculated. Different trial values of α_{eff} are used to fit the normalized temperature rise. The value giving the best fit is taken as the effective thermal diffusivity of the sample. For silk fibroin fiber sample (Type 2, before heat treatment), fitting of the experimental data is shown in Figure 1d. Its length is 0.61 mm, and the suspended sample is shown in Figure 1c. Its effective thermal diffusivity is determined at 8.24×10^{-7} m^2 s^{-1}, which includes the influence of the gold coating layer and radiation. For comparison, two curves of different α_{eff} values are also plotted in Figure 1d, one is $1.06\alpha_{eff}$ and the other is $0.94\alpha_{eff}$. It can be seen that by varying α_{eff} by 6%, the theoretical calculation deviates from the experimental data obviously. So the fitting uncertainty is about ±6%. Since the sample finally reaches the steady state, the overall temperature rise is

Table I Details of Experimental Parameters and Results for Silk Fibroin Fiber Sample (Type 2) Characterized by Using the TET and Calibration Technique

Sample	Type 2
Length (mm)	0.61
Average diameter (μm)	12.02
Cross-sectional area (μm^2)	113
DC current (mA)	0.7
Effective emissivity	0.92
Average resistance before heat treatment (Ω)	87.59
$\alpha_{real+radiation+gold}$ ($\times 10^{-7}$ m^2 s^{-1})	8.24
$\alpha_{real+\ radiation}$ ($\times 10^{-7}$ m^2 s^{-1})	5.38
α_{real} ($\times 10^{-7}$ m^2 s^{-1})	4.88
ρc_p ($\times 10^6$ J m^{-3} K^{-1})	1.35
Real thermal conductivity (W m^{-1} K^{-1})	0.66

the difference between the final temperature of the steady state and the initial temperature. The overall temperature rise in one heating period in Figure 1b can be calculated by $\Delta T = I^2 RL/(12kA)$ (detailed in work by Guo et al.[21]), where I is DC current, R the average resistance, k thermal conductivity, and L and A the length and cross-sectional area of the sample. For the fiber sample Type 2, the temperature rise is about 17.4°C in one heating period. Moreover, the temperature rise in the sample will not affect the properties of the silk since the DC square wave current is specially designed. It is long enough for the silk to reach the steady state when the current is on. Also the off-period is long for the sample to return to the initial temperature when the current is off. The DC current is applied for a very short time about 0.3 s as shown in Figure 1b for each heating cycle. In each measurement, the same heating circle is repeated 4–5 times to minimize possible experimental error/uncertainty and the whole measurement can be finished within several seconds.

After initial characterization, the sample is heated in the furnace at a certain temperature (about 140, 160, 180, and 220°C) for 30 min, cooled at the room temperature (about 22°C) for 30 min, and then placed in the vacuum chamber and characterized again. A scanning electron microscope (SEM) is used to study the dimensions (length and diameter) of the sample before and after heat treatment. Details about the experimental conditions and measurement results for silk fibroin fiber sample (type 2) are summarized in Table I. In this table, the effective emissivity and volume based specific heat (ρc_p) are the values we obtained from our previous work. According to Eqs. (3) and (4), after subtracting the gold and radiation effects, the real thermal diffusivity of the original silk fibroin fiber sample (Type 2) is 4.88×10^{-7} m^2 s^{-1}. Because the simple relationship between the thermal diffusivity and thermal conductivity can be expressed by $k = \alpha \rho c_p$, the silk's thermal conductivity is determined at 0.66 W m^{-1} K^{-1}. This high thermal conductivity is due to silk's highly ordered crystalline structures. For sheep wool, its thermal conductivity is only about 0.04–0.08 W m^{-1} K^{-1}. The thermal conductivity of human hair is about 0.24 W m^{-1} K^{-1} based on our studies.

Effect of Heat Treatment

The experimental results for silk fibroin fiber samples Types 1, 2, and 3 are shown in Table II and Figure 2 in detail. Because all of these samples are air-dried at 105°C for 2 h during initial preparation, so the thermal diffusivity and electrical resistance at 105°C (the first point of each curve in Figure 2) stand for the properties of the original samples before heat treatment. It is observed that the difference in the original thermal

Table II Details of Experimental Results for Silk Fibroin Fiber Samples Types 1, 2, and 3

Silk fibroin samples	Temperature (°C)	α_{real} ($\times 10^{-7}$ m^2 s^{-1})	Thermal diffusivity improvement	R_{start} (Ω)	R_{end} (Ω)
Type 1	105.0	4.77	0.0%	141.87	146.00
	143.3	5.79	21.4%	113.30	115.74
	166.4	6.58	37.9%	109.39	111.36
	189.8	5.72	19.9%	124.56	126.90
Type 2	105.0	4.88	0.0%	87.59	89.18
	140.1	5.77	18.2%	85.53	87.00
	160.7	5.84	19.7%	84.81	86.19
	187.2	5.80	18.9%	79.67	80.82
	209.8	5.90	20.9%	69.23	70.27
Type 3	105.0	4.18	0.0%	174.37	179.93
	142.2	4.57	9.3%	161.26	166.25
	166.7	4.54	8.6%	143.44	147.69
	190.6	5.08	21.5%	133.97	137.68
	220.0	4.85	16.0%	118.53	121.74

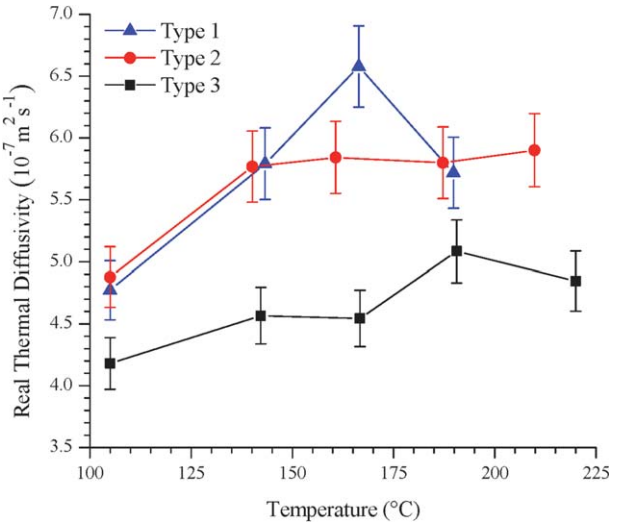

FIGURE 2 The real thermal diffusivity with 5% error bars of silk fibroin fiber samples Types 1, 2, and 3 before (105°C) and after heat treatment.

diffusivity among these samples is very small. These three different degumming methods do not result in significant thermal property difference between samples. From Figure 2a, it is apparent that, after heat treatment, the thermal diffusivity of Types 1, 2, and 3 silks has been significantly improved by 37.9% (heated at 166.4°C), 20.9% (heated at 209.8°C), and 21.5% (heated at 190.6°C), respectively. The increasing trend of these curves is similar. For Type 1 silk, it is very difficult to heat it at temperatures larger than 190°C without dramatically increasing the sample resistance to megaohm (electronically nonconductive). The thermal expansion of the fiber breaks the continuity of the gold film, and adhesion of the gold film is also weakened during heat treatment. This leads to an increase of the overall resistance, or just makes the sample not electrically conductive. For these three types of samples, a saturation point for thermal diffusivity increase is observed. The saturation point of thermal diffusivity increase is about 166, 140, and 190°C for Types 1, 2, and 3, respectively. After this point, further heat treatment at higher temperatures gives little thermal diffusivity increase or even decrease. In our experiment, a slight decrease of the electrical resistance after heat treatment is observed. Its effect on the overall thermal measurement has been subtracted precisely according to Eq. (4).

Sample Structural Change by Heat Treatment

In the past, thermomechanical analysis (TMA) has been applied to monitor the thermal expansion and contraction properties of silks.[7] The thermomechanical analysis curve of *Bombyx mori* silk fiber showed that, from room temperature to 120°C, the sample experienced a small contraction of about 0.7%. From 120 to 170°C, the sample length remained almost unchanged. Above 170°C, it began to expand slightly at a constant rate. The difference of the sample length at room temperature and 220°C is negligibly small.[7] We used SEM to check the diameter of the samples at the same location before and after heat treatment (at about 220°C). Figure 3 shows comparison of the diameter change of these samples. In fact, several locations are checked for each sample. For Type 1 sample, its average diameter increased by 0.44% after heat treatment at 220°C. For Type 2, the average diameter decreased by 1.29%. For Type 3, the average diameter increased by 0.19%. The sample dimension change by the heat treatment is very small and negligible considering the size measurement uncertainty under SEM. So it is reasonable to use the original diameter and length when calculating the cross-sectional area and subtracting gold and radiation effects during data processing for thermal diffusivity characterization.

For RSF films, Fourier transform infrared spectroscopy (FTIR) and Fourier self-deconvoluted (FSD) curve fitting are usually used to characterize the structural change (from amorphous to crystalline region) and calculate the crystalline degree induced by heat treatment, temperature-controlled water vapor annealing or exposure to chemicals.[2,12,13] Because the FTIR available to us has a spot size of 5 mm, it is too large for the diameter of the single silk fibroin fiber (about 10–20 μm). The signal is too weak to obtain effective FTIR spectrum. So in this work, Raman spectroscopy is performed for the same purpose. Raman spectra of the silk fibroin fibers before (105°C) and after (147 and 179°C) heat treatment are studied by using a confocal Raman spectrometer (Voyage, BWTek) coupled with an Olympus BX51 microscope. It employs a 532 nm green laser with 20 mW power as the excitation light source. The beam is focused with a 50× objective which gives a laser power about 8 mW on the sample. During the analysis, it is observed that the Raman intensity of samples heated at 179°C is very weak, thus cannot be effectively used to compare with that of original samples and samples heated at 147°C. The situation becomes even worse after the samples are heated above 179°C, and the laser can easily burn them.

Figure 4 shows the Raman study results before and after heat treatment at 147°C. There are several main peaks in the Raman spectrum which are related to β-sheets: Peaks 1 at 1081 cm^{-1} (νCC skeletal stretching, β-sheet); Peak 2 at 1230 cm^{-1} (amide III, β-sheet, δ CH_2 tw); and Peak 3 at 1665 cm^{-1} (amide I, νC=O in β-sheets).[26] All these three peaks for three types of fibers become sharper and narrower after heat treatment. In order to quantitatively study the peaks, the Raman peak linewidth: full width at half maximum (FWHM) is evaluated by using peak fitting. The difference of FWHM (FWHM before heat treatment minus that after heat treatment) for

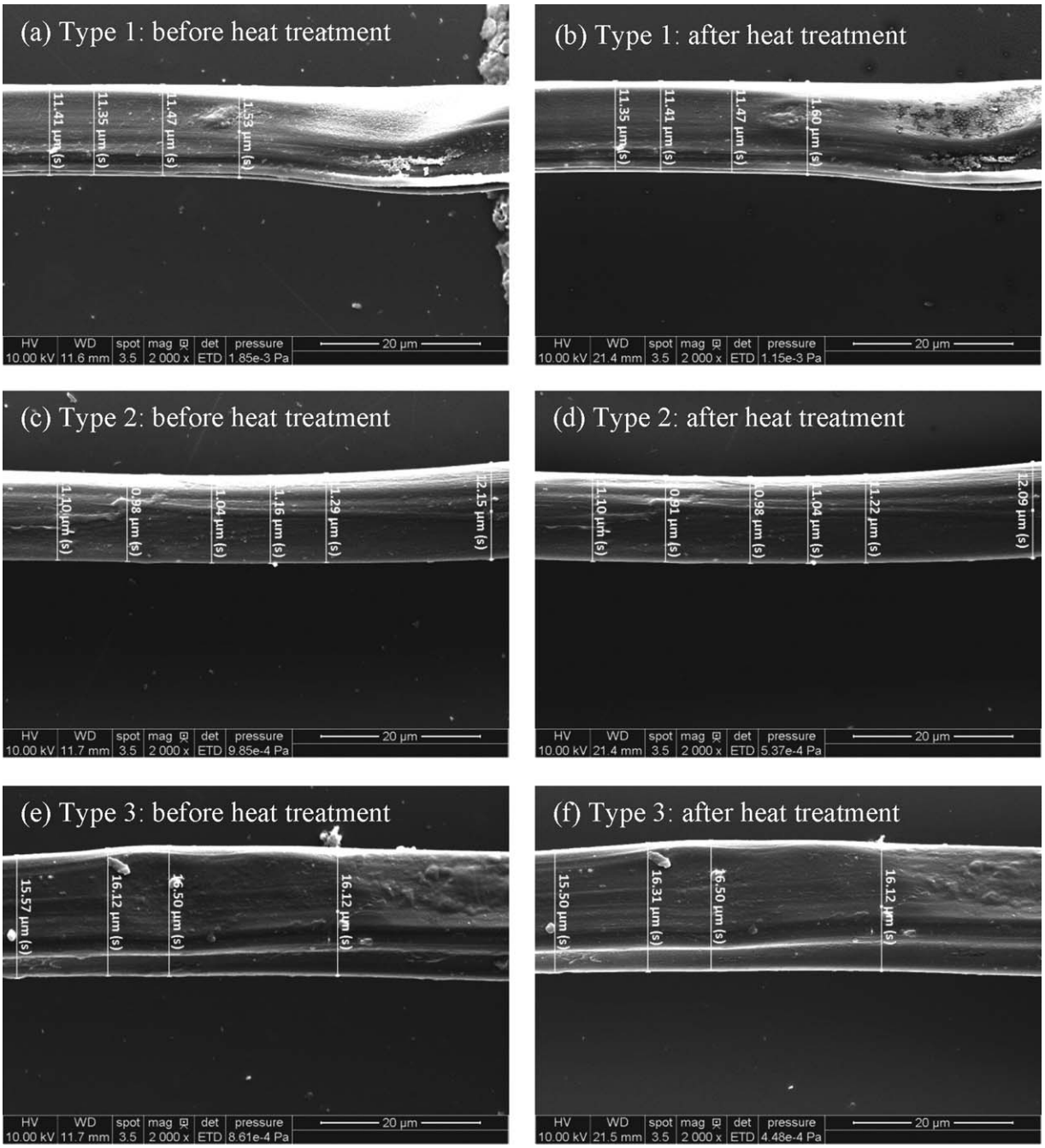

FIGURE 3 (a), (c), and (e) are SEM images of original (before heat treatment) silk fibroin fiber samples, Types 1, 2, and 3, respectively. (b), (d), and (f) are SEM images of heat treated (∼220°C) samples, Types 1, 2, and 3, respectively.

Peaks 1, 2, and 3 (Types 1, 2, and 3) is shown in Figure 4 (inset). Overall, Type 3 silk has the smallest linewidth reduction for the three peaks. For Types 1 and 2 silks, their linewidth reduction is small and close to each other at Peaks 1 and 2. At Peak 3, the linewidth is significantly reduced, around 9 cm^{-1} or larger. So the change in linewidth of Peak 3 (amide I, $\nu C{=}O$ in β-sheets) is coherent with the thermal diffusivity increase observed in Figure 2a. After the heat treatment at around 140°C, Types 1 and 2 samples have a large thermal diffusivity increase while Type 3 has a much smaller one. It is apparent that, after the heat treatment at 147°C, these peaks become stronger and sharper, which means the β-sheets

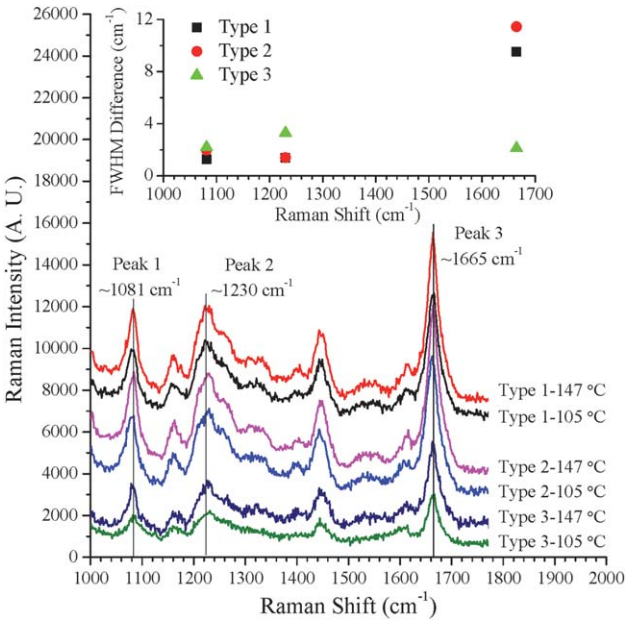

FIGURE 4 Raman analysis of silk fibroin fiber samples Types 1, 2, and 3 before (105°C) and after (147°C) heat treatment. The inset shows the difference of linewidth of Peaks 1, 2, and 3 before and after heat treatment.

(crystallinity degree) may be increased or the orientation of β-sheets with respect to the fiber axis is improved. Due to the fact that the laser used in this experiment is not polarized, so the chance for the latter mechanism is small.

A research group has done a full test (thermomechanical analysis, dynamic mechanical properties, X-ray diffraction and the refractive indices) of the structural changes of silk (*Bombyx mori* and *Antheraea pernyi*) fibers induced by heat treatment.[7] Though based on the x-ray diffraction curves, the crystalline structure of *Bombyx mori* silk fibers stayed unchanged after heat treatment. The isotropic refractive index (n_{iso}), which is related to the crystallinity of the fiber, did show a linear increase in the temperature range examined. A structure model, which is composed of amorphous, crystalline and laterally ordered regions, has been proposed to explain the structural changes induced by heat treatment. It is concluded in that work that, due to the close packing of the more adjacent laterally ordered regions, the number and size of the crystalline regions of *Bombyx mori* silk fibroin was increased by heat treatment.

For silk fibroin fibers naturally produced by silkworms, the crystallinity is approximately as high as 62–65%.[27] For RSF films of *Bombyx mori*, the crystallinity can be increased to 43% by heat treatment at 214°C, to 56% by exposing in methanol at room temperature for 4 days, and to 57.8–59.6% by water vapor annealing at 90–100°C.[2,12] It is apparent that, naturally produced fibroin fibers have the highest crystallinity. It is highly possible that, even being treated by various methods, the transformation from amorphous to crystalline structure though exists, but such transition should be very limited. Some references[2,28,29] also point out that, the X-ray diffraction analysis tends to be inaccurate at low crystalline fraction because many of the formed crystals are too small or imperfect to measurably contribute to the overall coherent scattering in the X-ray diffraction pattern. Although the X-ray diffraction did not detect the crystalline structural change of *Bombyx mori* silk fibers after heat treatment as reported in previous work, our Raman analysis did reveal that the peaks at 1081, 1230, and 1665 cm^{-1} becomes stronger and sharper. So we conclude that our observed thermal diffusivity increase by heat treatment is attributed to the following fact. Due to the close packing of the more adjacent laterally ordered regions, the number and size of the crystalline regions of *Bombyx mori* silk fibroin is increased by heat treatment. It is well known that the crystal phase is expected to have a higher thermal conductivity than the amorphous one.[30–33] Based on the fact that how difficult it is to characterize the tiny structural change precisely and how dramatically the thermal property changes by even small structural change, it leads to an important point that, thermal property characterization can be used to reflect the overall structural change of the protein fibers under various treatments. Additionally, we speculate that the heating treatment can induce breaking of the random H-bond in the nonrepetitive coil structures. It may reduce the phonon scattering among molecular chains and lead to an increased phonon mean free path. Therefore, the thermal transport capacity will increase, and the thermal diffusivity will increase as well.

Silkworm silk has a good ability of absorbing water. For RSF film, it generally contains 5–10% (w/w) water without humidity treatment.[10,15] For silk fiber naturally produced by silkworms, it has about 5% water.[9] When the temperature is lower than 100°C, which is the atmospheric boiling point of water, water may contribute significantly to the fluctuation of the thermal properties of different samples. For our silk fibroin fiber samples, the last step in original sample preparation is air drying them at 105°C for 2 h. Under this circumstance, the water effect on the thermal properties is suppressed significantly. In order to have a sense of the water effect on the samples, we characterized three groups of Type 1 samples (no heat treatment) using the TET technique, then soaked them in water for 30 min, air-dried them at room temperature for 30 min, and characterized them again. For Type 1 sample 1, the effective thermal diffusivity (includes gold and radiation effect) decreased by 9.31%; for Type 1 sample 2, increased by 10.97%; for Type 1 sample 3, increased by 1.25%. The changes of the effective thermal diffusivity do not have any trend, and could be induced by the gold film structure change by soaking and drying. The small water concentration change in the sample

has little effect on the thermal diffusivity. Therefore we conclude that the thermal diffusivity increase observed in Figure 2 is induced by the structure change/crystallinity increase rather than limited loss of the little water concentration in the silk.

CONCLUSION

In this work, the thermal transport capacity change induced by heat treatment in the axial direction of single filaments of silk (*Bombyx mori*) fibroin was investigated for the first time. The measured thermal diffusivity of the original silk fibroin fiber ranges from 4.18×10^{-7} to 4.88×10^{-7} m^2 s^{-1}. After heat treatment (from about 140°C to about 220°C), the thermal diffusivity of silk fibroin type 1, 2, and 3 increased by as high as 37.9%, 20.9%, and 21.5%, respectively. The SEM study revealed little change in the sample's dimension before and after heat treatment. This is consistent with the thermomechanical analysis curve from literature. Raman analysis revealed that after heat treatment at 147°C, the peaks at 1081, 1230, and 1665 cm^{-1} become stronger and narrower. This suggests structural transformation from amorphous to crystalline. A structure model that includes amorphous, crystalline and laterally ordered regions was proposed to explain the structural changes induced by heat treatment. Due to the close packing of the more adjacent laterally ordered regions, the number and size of the crystalline regions of *Bombyx mori* silk fibroin increased by heat treatment. As a result, the thermal diffusivity of the samples was significantly improved. Because of the high sensitivity of thermal property change by the structural change of silkworm silks, thermal characterization provides a very compelling way to uncover the overall structural change (crystalline degree or β-sheets content) of protein fibers.

Support of this work by the Army Research Office (W911NF-12-1-0272) and Office of Naval Research (N000141210603) is gratefully acknowledged. XW thanks the partial support of "Taishan Scholar" program of Shandong Province, China.

REFERENCES

1. Asakura, T.; Sugino, R.; Yao, J. M.; Takashima, H.; Kishore, R. Biochemistry US 2002, 41, 4415–4424.
2. Hu, X.; Kaplan, D.; Cebe, P. Macromolecules 2006, 39, 6161–6170.
3. Altman, G. H.; Diaz, F.; Jakuba, C.; Calabro, T.; Horan, R. L.; Chen, J. S.; Lu, H.; Richmond, J.; Kaplan, D. L. Biomaterials 2003, 24, 401–416.
4. Foo, C. W. P.; Kaplan, D. L. Adv Drug Deliv Rev 2002, 54, 1131–1143.
5. Demura, M.; Asakura, T.; Kuroo, T. Biosensors 1989, 4, 361–372.
6. Magoshi, J.; Magoshi, Y.; Nakamura, S.; Kasai, N.; Kakudo, M. J Polym Sci Pol Phys 1977, 15, 1675–1683.
7. Tsukada, M.; Freddi, G.; Nagura, M.; Ishikawa, H.; Kasai, N. J Appl Polym Sci 1992, 46, 1945–1953.
8. Martel, A.; Burghammer, M.; Davies, R. J.; Riekel, C. Biomacromolecules 2007, 8, 3548–3556.
9. Guan, J.; Porter, D.; Vollrath, F. Biomacromolecules 2013, 14, 930–937.
10. Hu, X.; Kaplan, D.; Cebe, P. Thermochim Acta 2007, 461, 137–144.
11. Hu, X.; Kaplan, D.; Cebe, P. Macromolecules 2008, 41, 3939–3948.
12. Zhu, G. B.; Wang, S. Y.; Feng, X. J.; Fan, G. N.; Jetten, M. S. M.; Yin, C. Q. Environ Sci Technol 2011, 45, 9951–9958.
13. Lu, Q.; Hu, X.; Wang, X. Q.; Kluge, J. A.; Lu, S. Z.; Cebe, P.; Kaplan, D. L. Acta Biomater 2010, 6, 1380–1387.
14. Liu, G.; Huang, X.; Wang, Y.; Zhang, Y.; Wang, X. Soft Matter 2012, 8, 9792–9799.
15. Motta, A.; Fambri, L.; Migliaresi, C. Macromol Chem Phys 2002, 203, 1658–1665.
16. Agarwal, N.; Hoagland, D. A.; Farris, R. J. J Appl Polym Sci 1997, 63, 401–410.
17. Magoshi, J.; Magoshi, Y.; Nakamura, S. Appl Polym Symp 1985, 187–204.
18. Hu, X.; Lu, Q.; Kaplan, D. L.; Cebe, P. Macromolecules 2009, 42, 2079–2087.
19. Cebe, P.; Hu, X.; Kaplan, D. L.; Zhuravlev, E.; Wurm, A.; Arbeiter, D.; Schick, C. Sci Rep-Uk 2013, 3, 1130.
20. Zheng, Y. M.; Bai, H.; Huang, Z. B.; Tian, X. L.; Nie, F. Q.; Zhao, Y.; Zhai, J.; Jiang, L. Nature 2010, 463, 640–643.
21. Guo, J. Q.; Wang, X. W.; Wang, T. J Appl Phys 2007, 101, 063537.
22. Chen, H. Y.; Xue, D. S.; Feng, X. Y.; Yao, S. J. Appl Biochem Biotech 2011, 165, 1754–1769.
23. Feng, X.; Wang, X.; Chen, X.; Yue, Y. Acta Mater 2011, 59, 1934–1944.
24. Guo, J. Q.; Wang, X. W.; Zhang, L. J.; Wang, T. Appl Phys A Mater 2007, 89, 153–156.
25. Lin, H.; Xu, S.; Li, C.; Dong, H.; Wang, X. Nanoscale 2013, 5, 4652–4656.
26. Colomban, P.; Dinh, H. M.; Riand, J.; Prinsloo, L. C.; Mauchamp, B. J Raman Spectrosc 2008, 39, 1749–1764.
27. Warwicker, J. O. J Mol Biol 1960, 2, 350–362.
28. Asakura, T.; Kuzuhara, A.; Tabeta, R.; Saito, H. Macromolecules 1985, 18, 1841–1845.
29. Um, I. C.; Kweon, H. Y.; Park, Y. H.; Hudson, S. Int J Biol Macromol 2001, 29, 91–97.
30. Yamasaki, M.; Kagao, S.; Kawamura, Y. Script Mater 2005, 53, 63–67.
31. Huang, Z. X.; Tang, Z. A.; Yu, J.; Bai, S. Y. Phys B 2009, 404, 1790–1793.
32. Nath, P.; Chopra, K. L. Phys Rev B 1974, 10, 3412–3418.
33. Shukla, N. C.; Liao, H. H.; Abiade, J. T.; Liu, F. X.; Liaw, P. K.; Huxtable, S. T. Appl Phys Lett 2009, 94, 081912.

Reviewing Editor: Kenneth J. Breslauer